Observation of the second harmonic in superconducting current-phase relation of Nb/Au/(001)YBa$_2$Cu$_3$O$_x$ heterojunctions

P. V. Komissinski (*)[1,3], E. Il'ichev[2], G. A. Ovsyannikov[3], S. A. Kovtonyuk[3], M. Grajcar[4], R. Hlubina[4], Z. Ivanov[1], Y. Tanaka[5], N. Yoshida[5] and S. Kashiwaya[6]

[1] *Department of Microelectronics and Nanoscience, Chalmers University of Technology and Göteborg University, S-412 96, Göteborg, Sweden*
[2] *Institute for Physical High Technology, Dept. of Cryoelectronics, P.O. Box 100239, D-07702 Jena, Germany*
[3] *Institute of Radio Engineering and Electronics, RAS, Moscow 101999, Russia*
[4] *Department of Solid State Physics, Comenius University, Mlynská Dolina, SK-842 48 Bratislava, Slovakia*
[5] *Department of Applied Physics, Nagoya University, 464-8603, Nagoya, Japan*
[6] *Electrotechnical Laboratory, Umezono, Tsukuba, Ibaraki, 305-8568, Japan*

Abstract. – The superconducting current-phase relation (CPR) of Nb/Au/(001)YBa$_2$Cu$_3$O$_x$ heterojunctions prepared on epitaxial c-axis oriented YBa$_2$Cu$_3$O$_x$ thin films has been measured in a single-junction interferometer. For the first time, the second harmonic of the CPR of such junctions has been observed. The appearance of the second harmonic and the relative sign of the first and second harmonics of the CPR can be explained assuming, that the macroscopic pairing symmetry of our YBa$_2$Cu$_3$O$_x$ thin films is of the $d + s$ type.

Introduction. It is now well established that the dominant component of the superconducting order parameter in the cuprates has d-wave symmetry (see [1] and references therein). Moreover, it has become clear that in orthorhombic materials such as YBa$_2$Cu$_3$O$_x$ (YBCO), a finite component with s-wave symmetry is admixed to the dominant d-wave order parameter. The early in-plane phase sensitive experiments imply that the d-wave component remains coherent through the whole sample [1], while an elegant c-axis tunneling experiment shows directly that the s-wave order parameter component does change sign across the twin boundary [2].

The above picture of the YBCO pairing state is challenged by the experimental observation of a finite c-axis Josephson current between heavily twinned YBCO and a Pb counterelectrode [3]. Namely, the contribution of the s-wave part of the YBCO order parameter to

---

(*) Corresponding author. E-mail adress: filipp@fy.chalmers.se <mailto:filipp@fy.chalmers.se>

the Josephson coupling between a conventional superconductor (superconductor with a pure s-wave symmetry of the order parameter, for example Pb or Nb) and YBCO should average to zero for equal abundances of the two types of twins in YBCO. In other words, the macroscopic pairing symmetry of twinned YBCO samples should be a pure d-wave [4]. Tanaka has shown that a finite second order Josephson current obtains for a junction between the s-wave and c-axis oriented pure d-wave superconductors [5]. However, measurements of microwave induced steps at multiples of $hf/2e$ on the I-V curves of Pb/Ag/YBCO tunnel junctions imply dominant first order tunneling [6]. Therefore the finite c-axis Josephson current has to result from a nonvanishing admixture of the s-wave component to the macroscopic order parameter of YBCO [4]. Two alternatives of how this can take place in the junctions based on twinned YBCO have been discussed in the literature:

(i) Sigrist *et al.* have suggested that the phase of the s-wave component in YBCO does not simply jump from 0 to π upon crossing the twin boundary, but rather changes in a smooth way, attaining the value of $\pi/2$ right at the twin boundary [7]. The twinned YBCO sample is thus assumed to exhibit a macroscopic $d + is$ pairing symmetry. A related picture has been proposed by Haslinger and Joynt, who suggest a $d + is$ surface state of YBCO [8].

(ii) A difference in the abundances of the two types of twins implies a $d + s$ symmetry of the macroscopic pairing state [9]. Let us point out that also structural peculiarities of other type (such as a lamellar structure in a preferred direction) may lead to the $d + s$ macroscopic pairing symmetry.

In this paper we report the observation of a large second harmonic of the Josephson current in Nb/Au/(001)YBCO junctions. By comparing the relative signs of the first and second harmonics of the Josephson current, we show that the macroscopic $d + s$ pairing symmetry is realized in our YBCO samples. Our results might be relevant also in search for so called "quiet" qubits which can be realized making use of junctions with a dominant second harmonic of the Josephson current [10]. Another promising route to fabricate such junctions is via 45° grain boundary Josephson junctions [11, 12].

Experimental. In realization of the Josephson junctions between conventional superconductors and c-axis oriented high-temperature ones an extensive use has been made of the Pb/Ag/(001)YBCO heterojunctions [3]. In search for a combination of the superconducting counterelectrode and a normal-metal buffer layer with the highest possible interface quality, in the present work we have decided to study the Nb/Au/(001)YBCO heterojunction. Our epitaxial (001)-oriented YBCO films with thicknesses of 150 nm were obtained by laser deposition on (100) LaAlO$_3$ and (100) SrTiO$_3$ substrates. The films are usually twinned in the ab-plane. The superconducting transition temperature of our YBCO films was determined by magnetic susceptibility measurements as $T_c = 88 \div 90$ K. The YBCO films were *in situ* covered by a $8 \div 20$ nm thick Au layer, thus preventing the degradation of the YBCO surface during processing. Afterwards, 200 nm thick Nb counterelectrodes were deposited by DC-magnetron sputtering. Photolithography and low energy ion milling techniques were used to fabricate the Nb/Au/YBCO junctions. The interface resistance per unit area $R_B = R_N S$ (where R_N is the normal state resistance and S is the junction area) was $R_B = 10^{-5} \div 10^{-6}$ $\Omega \cdot$cm^2. Details of the junction fabrication were reported elsewhere [13].

Surface quality of the YBCO films is very important when current transport in the c-axis direction is investigated. High-resolution atomic force microscopy reveals a smooth surface consisting of approximately 100 nm long islands with vertical peak-to-valley distance of ≈ 3 nm (fig. 1). We can exclude that substantial ab-plane tunnel currents flow between YBCO and Nb at the boundaries of these islands. In fact, theory predicts formation of midgap states at the surface of semi-infinite CuO$_2$ planes [14, 15]. Therefore zero bias conductance peaks should be expected in the I-V characteristics at temperatures larger than the critical temperature

of Nb, if the contribution of *ab*-plane tunneling was nonnegligible. However, no such peaks have been observed for all fabricated Nb/Au/YBCO junctions. Moreover, from the size of the islands and from the vertical peak-to-valley distance we estimate that the area across which *ab*-plane tunneling might take place is less than 6% of the total junction area. Since the interface resistances per square are of the same order of magnitude [3] for both, the *c*-axis and *ab*-plane junctions, we conclude that *ab*-plane tunneling from YBCO, if present, is negligibly small.

We have measured more than 20 single junctions with areas in the range from $10 \times 10 \ \mu\mathrm{m}^2$ to $100 \times 100 \ \mu\mathrm{m}^2$. At small voltages the typical *I-V* curves can be described by the resistively shunted junction model with a small McCumber parameter [16]. Typical critical current densities were $j_c = 1 \div 12 \ \mathrm{A/cm}^2$ and $j_c R_B = 10 \div 90 \ \mu\mathrm{V}$. The differential resistance *vs.* voltage dependence $R_d(V)$ exhibits a gap-like structure at $V \approx 1.2$ mV at $T = 4.2$ K (see fig. 2). This structure has a BCS-like temperature dependence and disappears at $T_{cR} \approx 9.1$ K, therefore we ascribe it to the superconducting energy gap of Nb.

The CPR measurements were performed using a single-junction interferometer configuration in which a junction of interest is inserted into a superconducting loop with an inductance $L \approx 80$ pH. We measure the impedance of a parallel resonance circuit inductively coupled to the interferometer as a function of the external magnetic flux Φ_e threading the interferometer. The dimensionless CPR $f(\varphi) = I_s(\varphi)/I_c$ (where $I_s(\varphi)$ is the Josephson current) can be extracted from the following equations:

$$\varphi = \varphi_e - \beta f(\varphi), \tag{1}$$

$$\tan \alpha = \frac{k^2 Q \beta f'(\varphi)}{1 + \beta f'(\varphi)}, \tag{2}$$

where $\varphi_e = 2\pi \Phi_e / \Phi_0$, φ is the phase difference across the Josephson junction, the prime denotes a derivative with respect to φ, α is the phase shift between the driving current and the tank voltage at the resonant frequency, $\beta = 2\pi L I_c / \Phi_0$ is a normalized critical current, Q is the quality factor of the parallel resonance circuit, k is the coupling coefficient between the RF SQUID and the tank coil, and Φ_0 is the flux quantum. This method, being differential with respect to φ, provides a high sensitivity of the CPR measurement. Moreover, $I_s(\varphi)$ is measurable even if the thermal energy exceeds the Josephson coupling energy. In fact, critical currents down to 50 nA were recently detected at $T = 4.2$ K [17].

For the junction SQ10, β varied between 0.4 and 0.27 for temperatures in the range $T = 1.7 \div 6.0$ K. Since $\beta < 1$, we can extract the CPR from the $\alpha(\varphi_e)$ dependence for the complete phase range (see figs. 3 and 4). Fourier analysis of the experimentally obtained CPR shows substantial first and second harmonics and negligibly small higher-order harmonics. Therefore we can write

$$I_s(\varphi) = I_1 \sin \varphi + I_2 \sin 2\varphi \tag{3}$$

for all temperatures below the transition temperature of Nb. The sign of I_2 is always opposite to that of I_1. In what follows we use the convention that $I_1 > 0$ and therefore $I_2 < 0$. The ratio $|I_2/I_1|$ grows with decreasing temperature reaching $|I_2/I_1| \approx 0.16$ at $T \approx 1.7$ K, when $I_1 = 1.57 \ \mu\mathrm{A}$ and $I_2 = -0.25 \ \mu\mathrm{A}$ (see inset to a fig. 4).

We point out that the main result of this paper, namely the large negative value $I_2/I_1 \approx -0.16$ observed at low temperatures, is not the result of an indirect data analysis, but it follows directly from the measured $\alpha(\varphi_e)$ dependences. In fact, one finds readily that

$$\frac{d^2 \tan \alpha}{d\varphi_e^2} = \frac{k^2 Q \beta f'''}{(1 + \beta f')^4}, \tag{4}$$

where all derivatives are taken at $\varphi = 0$ or $\varphi_e = 0$. Thus, the existence of the local minima of $\alpha(\varphi_e)$ at multiples of π dictates that $f''' > 0$, or, making use of Eq. (3), $I_2/I_1 < -1/8$. Note that neither the conventional tunneling theory nor the I and II theories by Kulik and Omelyanchuk predict such local minima on the derivatives of CPR [16].

Discussion. Let us estimate the transparency of the barrier between YBCO and Nb from the normal-state resistance per unit area R_B. According to the band-structure calculations (for a review, see [18]), the hole Fermi surface of YBCO is a slightly warped barrel with an approximately circular in-plane cross-section (to be called Fermi line) with radius k_F. In what follows, we represent the electron wavevector $\mathbf{k}$ in cylindrical coordinates, $\mathbf{k} = (k, \theta, k_z)$. We estimate the uncertainty of the in-plane momentum as $\delta k \approx 2\pi/l$, where l is the characteristic size of the islands on the YBCO surface (fig.1). We evaluate R_B making use of the Landauer formula and note that only tunneling from a shell around the Fermi line with width δk is kinematically allowed. The barrier transparency $D(\theta)$ depends on the details of the c-axis charge dynamics in YBCO, with maxima in those directions θ, in which the YBCO c-axis Fermi velocity $w(\theta)$ is maximal. Since for $\theta = \pi/4$ and symmetry equivalent directions $w(\theta)$ is minimal [19], we expect that there will be 8 maxima of $D(\theta)$ on the YBCO Fermi line where $D(\theta) \approx D$, which are situated at $\theta = \theta_0$ and symmetry equivalent directions. The modulation of the function $D(\theta)$ depends on the thickness of the barrier between YBCO and Nb [20]. We consider two limiting distributions of the barrier transparency $D(\theta)$ along the YBCO Fermi line: (a) a featureless $D(\theta) \approx D$ and (b) a strongly peaked $D(\theta)$, roughly corresponding to thin and thick barriers, respectively [20]. In the thick barrier limit the angular size of the maxima of $D(\theta)$ can be estimated as $\delta\theta \approx \delta k/k_F$. With these assumptions we find

$$R_B^{-1} = \frac{\langle D \rangle e}{\Phi_0} A, \tag{5}$$

where A measures the number of conduction channels and $\langle \ldots \rangle$ denotes an average over the junction area. In the thin and thick barrier limits, we find $A \approx k_F \delta k/\pi$ and $A \approx 2\delta k^2/\pi$, respectively. Taking $l \approx 100$ nm and $k_F \approx 0.6$ Å^{-1} [21], the measured $R_B = 6 \times 10^{-5}$ Ωcm^2 of the junction SQ10 can be fitted with $\langle D \rangle_{\text{thin}} \approx 1.7 \times 10^{-5}$ and $\langle D \rangle_{\text{thick}} \approx 8.3 \times 10^{-4}$.

Since we have observed no midgap surface states in the $R_d(V)$ curves, we can neglect the surface roughness, and the Josephson current can be calculated from [22]

$$I_s(\varphi) = \frac{2e}{\hbar} \sum_{k,\theta} k_B T \sum_{\omega} \frac{D \Delta_R \Delta_{\mathbf{k}} \sin\varphi}{2\Omega_R \Omega_{\mathbf{k}} + D\left[\omega^2 + \Omega_R \Omega_{\mathbf{k}} + \Delta_R \Delta_{\mathbf{k}} \cos\varphi\right]}, \tag{6}$$

where the sum over k, θ is taken over the same regions with areas A as in Eq. (5), Δ_R and $\Delta_{\mathbf{k}}$ are the Nb and YBCO gaps, respectively, and $\Omega_i = \sqrt{\omega^2 + \Delta_i^2}$ with $i = R, \mathbf{k}$. Keeping only terms up to second order in the (small) junction transparency D, the Josephson current densities $j_i = I_i/S$ read

$$j_1(T) R_B \approx \frac{\Delta_s}{\Delta_d^*} \frac{\Delta_R(T)}{e}, \tag{7}$$

$$j_2(T) R_B \approx -\frac{\pi}{8} \frac{\langle D^2 \rangle}{\langle D \rangle} \frac{\Delta_R(T)}{e} \tanh\left(\frac{\Delta_R(T)}{2k_B T}\right), \tag{8}$$

where $\Delta_d^* = \pi \Delta_d [2\ln(3.56\Delta_d/T_{cR})]^{-1}$ and $\Delta_d^* = \Delta_d |\cos 2\theta_0|$ in the thin and thick barrier limits, respectively. In Eqs. (7,8) we used the YBCO gap $\Delta(\theta) = \Delta_s + \Delta_d \cos 2\theta$, where Δ_d and Δ_s are the d-wave and s-wave gaps. We have assumed that Δ_d^* is larger than both, Δ_R and Δ_s. The factor Δ_s/Δ_d^* can be estimated from the measured $j_1 R_B$ products for

Josephson junctions between untwinned YBCO single crystals and Pb counterelectrodes. For such junctions $j_1(0)R_B \approx 0.5 \div 1.6$ meV [3]. Using the Pb gap $\Delta_R = 1.4$ meV in Eq. (7), we obtain $\Delta_s/\Delta_d^* \approx 0.36 \div 1.1$.

Note that within the above microscopic $d+s$ scenario, the signs of I_1 and I_2 are different. This feature remains valid also in the macroscopic $d+s$ scenario, whereas within the macroscopic $d+is$ picture, the same signs of I_1 and I_2 are expected. Thus we conclude that the finite first harmonic has to be due to the macroscopic $d+s$ symmetry of our YBCO sample. In fact, detailed structural studies show that for sufficiently thin YBCO films, the abundances of the two types of twins can be different even for films grown on the cubic substrate SrTiO$_3$ [23]. If we denote the twin fractions as $(1+\delta)/2$ and $(1-\delta)/2$, then the measured first harmonic of the CPR, $\langle j_1 \rangle$, is proportional to the deviation from equal population of twins, $\langle j_1 \rangle = \delta j_1$ [9]. Using $\Delta_R = 1.2$ meV determined from the $R_d(V)$ data and our estimate $\Delta_s/\Delta_d^* \approx 0.36 \div 1.1$, we find that the measured first harmonic $\langle j_1 \rangle$ for the junction SQ10 can be fitted with $\delta \approx 0.07 \div 0.21$, which is in qualitative agreement with [23], where $\delta \approx 0.14$ for 1000 Å thick YBCO films has been observed.

Fitting the measured $j_2 R_B$ of the junction SQ10 by Eq. (8) we obtain $\langle D^2 \rangle/\langle D \rangle \approx 3.2 \times 10^{-2}$, which is much larger than both $\langle D \rangle_{\text{thin}}$ and $\langle D \rangle_{\text{thick}}$. This diference can be explained provided the junction transparency D is a fluctuating function of the position $\mathbf{r}$. In fact, adopting the WKB description of tunneling [20], we write $D(s(\mathbf{r})) = \exp(-s_0 - s(\mathbf{r}))$, where s_0 is the WKB tunneling exponent and $s(\mathbf{r})$ its local deviation from the mean. Assuming a Gaussian distribution of s with a mean deviation η, $P(s) \propto \exp(-s^2/\eta^2)$, we estimate the spatial averages as $\langle D^n \rangle = \int_{-s_0}^{s_0} ds P(s) D^n(s)$. In the thin barrier limit, the values $\langle D^2 \rangle_{\text{thin}} = 8.6 \times 10^{-7}$ and $\langle D \rangle_{\text{thin}} = 2.3 \times 10^{-5}$ required to fit the experiments correspond to an average WKB exponent $s_0^{\text{thin}} \approx 15.5$ with $\eta_{\text{thin}} \approx 4.3$. In the thick barrier limit we obtain $s_0^{\text{thick}} \approx 9.1$ and $\eta_{\text{thick}} \approx 2.8$. We would like to emphasize that, because of it's stochastic origin, the ratio I_2/I_1 is hard to control experimentally. This explains why only 2 out of 7 measured samples exhibited a measurable second harmonic.

Let us consider also the second harmonic generation by a mechanism proposed by Millis for planar junctions [24]. We can view the junction as a checkerboard of 0 and π junctions with a lattice constant a (characteristic size of an YBCO twin) and local critical current density j_1. As shown by Millis, spontaneous currents are generated in the ground state of such a junction and the junction energy is minimized for the phase difference $\pm\pi/2$. An explicit calculation in the limit $a, \lambda_R \ll \lambda \ll \lambda_c$ (where λ, λ_c are the ab-plane and c-axis penetration depths of YBCO and λ_R is the Nb penetration depth) yields

$$j_{2,\text{Millis}} \approx -\frac{1}{4\sqrt{2}} \frac{\mu_0 j_1^2 a \lambda \lambda_c}{\Phi_0}.$$

Comparing $j_{2,\text{Millis}}$ with Eq. (8), we find

$$\frac{j_{2,\text{Millis}}}{j_2} \approx \frac{8\sqrt{2}F}{\pi^2} \left(\frac{\Delta_s}{\Delta_d^*} \right)^2 \frac{a}{l} \frac{\Delta_R}{\hbar c/\lambda_c} \frac{E_0}{\hbar c/\lambda},$$

where $E_0 = e^2 q_0/4\pi\epsilon_0$ with $q_0 = k_F$ and $2\delta k$ for a thin and thick barrier, respectively. F depends on the characteristic length scale L of the fluctuations of the junction transparency: for $L \ll a$, $F \approx \langle D \rangle^2/\langle D^2 \rangle$, whereas for $L \gg a$, $F \approx 1$. In order to estimate the upper bound of the ratio $j_{2,\text{Millis}}/j_2$, we consider the thin barrier limit, take $F \approx 1$, $\Delta_s/\Delta_d^* \approx 1.1$, $a \approx 10$ nm, $\lambda \approx 240$ nm, and $\lambda_c \approx 3$ μm (the last two values are valid for underdoped YBCO [25]) and we find that $j_{2,\text{Millis}}/j_2 < 0.03$. Thus we can safely neglect the contribution of the Millis mechanism to the second harmonic of the CPR.

Conclusion. We have observed the second harmonic I_2 of the current-phase relation in c-axis Nb/Au/YBCO heterojunctions. We have shown that the relative phases of the first and second harmonics of the CPR together with their amplitudes I_1 and I_2 and the normal-state resistance of the Josephson junctions observed in the experiment can be explained making use of a single set of parameters within the standard microscopic $d + s$ picture of the YBCO pairing state, assuming the difference in the abudances of the two types of twins and that the barrier fluctuates along the junction.

<p align="center">* * *</p>

REFERENCES

[1]   Tsuei C. C. and Kirtley J. R., *Rev. Mod. Phys.*, **72** (2000) 969.
[2]   Kouznetsov K. A. *et al.*, *Phys. Rev. Lett.*, **79** (1997) 3050.
[3]   Sun A. G. *et al.*, *Phys. Rev. B*, **54** (1996) 6734.
[4]   Walker M. B. and Luettmer-Strathmann J., *Phys. Rev. B*, **54** (1996) 588.
[5]   Tanaka Y., *Phys. Rev. Lett.*, **72** (1994) 3871.
[6]   Kleiner R. *et al.*, *Phys. Rev. Lett.*, **76** (1996) 2161.
[7]   Sigrist M. etal, *Phys. Rev. B*, **53** (1996) 2835.
[8]   Haslinger R. and Joynt R., *J. Phys.: Condens. Matter*, **12** (2000) 8179.
[9]   O'Donovan C. *et al.*, *Phys. Rev. B*, **55** (1997) 9088.
[10] Ioffe L. B. *et al.*, *Nature*, **398** (1999) 679.
[11] Il'ichev E. *et al.*, *Phys. Rev. B*, **60** (1999) 3096.
[12] Il'ichev E. *et al.*, *Phys. Rev. Lett.*, **86** (2001) 5369.
[13] Komissinskii F. V. *et al.*, *JETP*, **89** (1999) 1160.
[14] Hu C., *Phys. Rev. Lett.*, **72** (1994) 1526.
[15] Tanaka Y. and Kashiwaya S., *Phys. Rev. Lett.*, **74** (1995) 3451.
[16] Likharev K. K., *Rev. Mod. Phys.*, **51** (1979) 101.
[17] Ilichev E. *et al.*, *Rev. Sci. Instr.*, **72** (2001) 1882.
[18] Pickett W. E., *Rev. Mod. Phys.*, **61** (1989) 433.
[19] Xiang T. and Wheatley J. M., *Phys. Rev. Lett.*, **77** (1996) 4632.
[20] Wolf E. L., *Principles of Electron Tunneling Spectroscopy* (Oxford University Press, New York) 1985
[21] Shen Z. X. and Dessau D., *Physics Reports*, **253** (1995) 1.
[22] Zaitsev A. V., *Sov. Phys. JETP*, **59** (1984) 1015.
[23] Didier N. *et al.*, *J. of Alloys and Compounds*, **251** (1997) 322.
[24] Millis A. J., *Phys. Rev. B*, **49** (1994) 15408.
[25] Cooper S. L. and Gray K. E., *in: Physical Properties of High Temperature Superconductors*, Vol. **IV** (Ed. D. M. Ginsberg, World Scientific, Singapore) 1994.

Figure captions

Fig. 1. Left panel: A high resolution AFM image of the surface of a 150 nm thick YBCO film. Right panel: Height profile of the YBCO surface along the line indicated in the left panel. The peaks and valleys are shown by markers. The peak-to-valley distance is ≈ 3 nm and about 100 nm in the vertical and horisontal directions respectively.

Fig.2(a) Typical $I - V$ curve and (b) differential resistance vs. voltage dependence $R_d(V)$ of a Nb/Au/YBCO junction with a 20 nm thick Au film, measured at $T = 4.2$ K. The low voltage part of the $I - V$ curve ($V \leq 0.3$ mV) is shown on the inset.

Fig. 3. Phase shift α as a function of φ_e for the junction SQ10 at $T =$1.7, 2.5, 3.5, 4.2, and 6.0 K (from bottom to top).

Fig. 4. The current-phase relation $I(\varphi)$ of the junction SQ10 at T=1.7, 2.5, 3.5, 4.2, and 6.0 K (from top to bottom). Inset: Temperature dependence of I_1 (squares) and $|I_2|$ (circles). Solid lines are fits to Eqs. (7,8) using $\Delta_R(T) = \Delta_R(0) \tanh[\Delta_R(T)T_{cR}/\Delta_R(0)T]$.
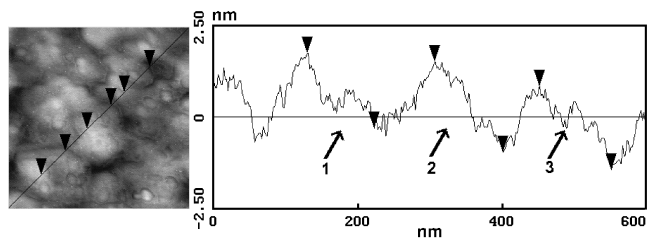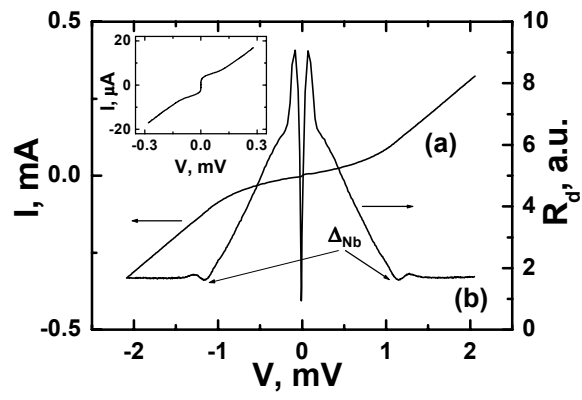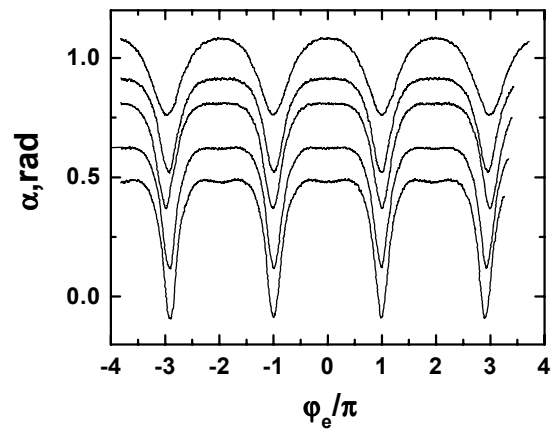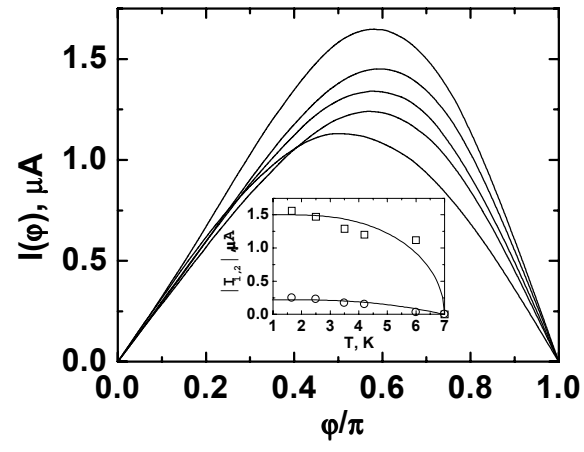
Fig. 1

Fig. 2

Fig. 3

Fig. 4.